Hydraulic Model Experiment Involving Tidal Motion

Part III. Experimental Result and Theoretical Consideration

1. Introduction

On the point of view for the similitude as stated above, the experiments involving tidal motion were carried out in both cases, that is, the flow in the model belonged to the laminar regime and transient regime. To confirm the similitude, the area which had been investigated in some detail was chosen as the prototype. A part of Hiroshima Bay was chosen as the prototype in the case of the laminar regime. The experiment for this prototype is called in the following as experiment for bay model. The reason why this region was chosen was that, since Inland Sea Fisheries Research Institute had previously investigated this area in detail, it was thought to be convenient to obtain the data for the prototype. Moreover, a training dyke of 1.5 km long was being planned at the right bank of Fukushima River which empties into this sea area, so it will be interesting to see what change may take place in the future in the state of the sea by this construction.

As the prototype in the case of transient regime, Sakai Channel was chosen. Because, various investigation had been done in this area by Ministry of Agriculture and Forestry, Ministry of Transportation, Government of Shimane Prefecture and Tottori Prefecture, prior to execute the plan to close the channel in view of making the water of Nakaumi fresh by the inflow of rivers into it as the first step of the reclamation work in Nakaumi, which is connected with Miho Bay through this channel. The experiment for this prototype is called experiment for inlet model.

2. Experiment for bay model

1. Prototype

The area chosen as prototype was the northern part of Hiroshima Bay and involved the mouth of Fukushima River. The area involved in the model is shown in Fig. 4. The field observations of tidal current were done when the velocity attained maximum value both in flood and ebb tide from May

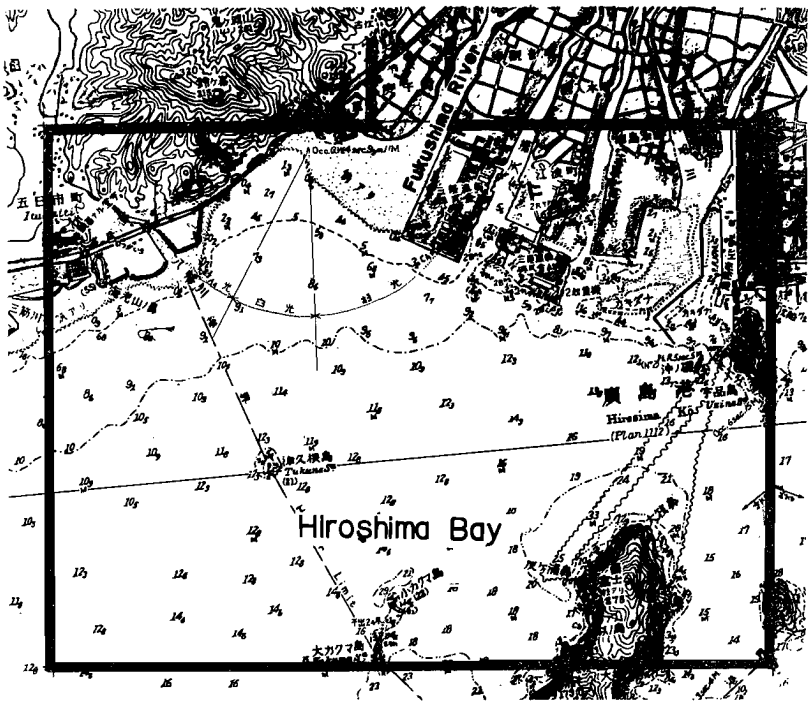

Fig. 4. Prototype of the bay model.

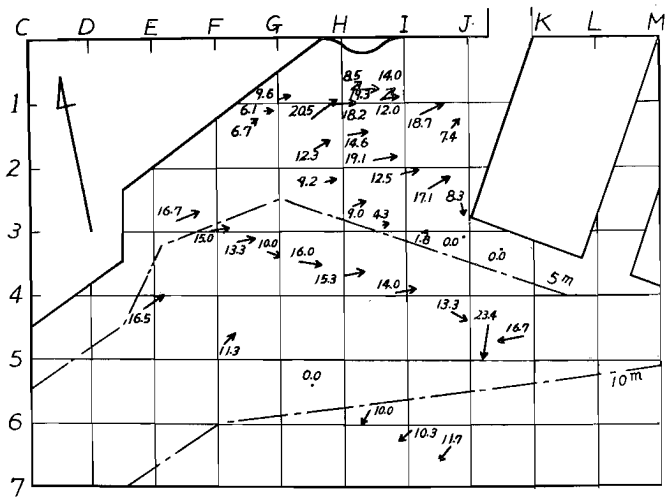

Fig. 5. Pattern of the maximum flood current. Prototype May 16, 1957.

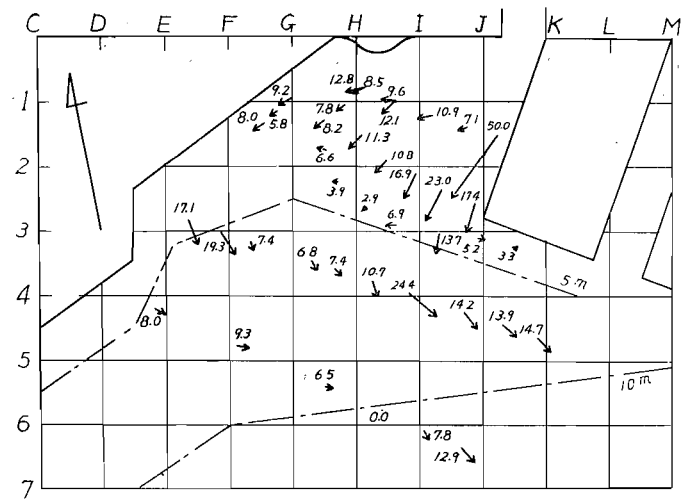

Fig. 6. Pattern of the maximum ebb current. Prototype May 16, 1957.

Table 1. Direction and velocity of wind at Hiroshima Meteorological Station, May 16, 1957.

Time (hr)	1	2	3	4	5	6	7	8	9	10	11	12	13	14	15	16
Direction	NNE	〃	〃	〃	〃	〃	〃	〃	〃	〃	S	SSW	SW	〃	〃	SSW
Velocity (m/sec)	5.5	6.1	6.5	7.6	5.7	5.7	5.4	3.6	2.4	2.8	4.6	1.3	4.2	1.3	4.2	3.8

Time (hr)	17	18	19	20	21	22	23	24
Direction	SW	〃	〃	〃	NNE	〃	〃	〃
Velocity (m/sec)	3.6	1.3	4.8	0.2	2.6	4.6	3.8	4.0

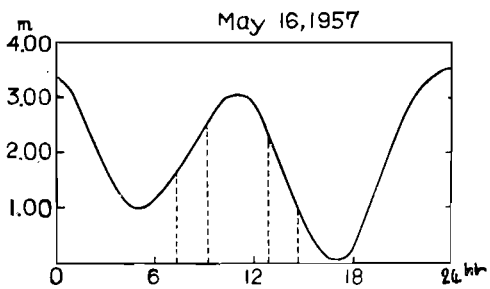

Fig. 7. Tidal curve in Hiroshima Bay. Periods of current observation are indicated by broken lines.

14 to 16, 1957. Many observation stations were set in this area and the velocities and directions of flow at the depth of 50 cm below the sea surface were measured. Because of the effect of the wind, the results of the observations were not the same. The results on May 16, when it was comparatively calm, are shown in Fig. 5 and 6. The wind observed at Hiroshima Weather Bureau on that day is given in Table 1. The tidal curve on that day is shown in Fig. 7, where the times

of observation are shown in broken line (at flood ; 07.20~09.10, at ebb ; 12.50 ~14.40). As shown in these figures, the current velocity is generally weak and seldom exceeds 20 cm/sec. Especially remarkable is the fact that, near the contour-line of 5 m, the velocities are very weak both at flood and ebb. Inside this contour-line the water depth decreases rapidly to 2 m or less, while in the outer part of this it increases rapidly.

2. Procedure of the experiment

The model was constructed for this prototype. Considering the area of the prototype and the dimentions of the basin, the horizontal scale x_r was decided as 500. The breadth of the basin was 20 m so that it contained the coast of about 10 km in the prototype (Fig. 8).

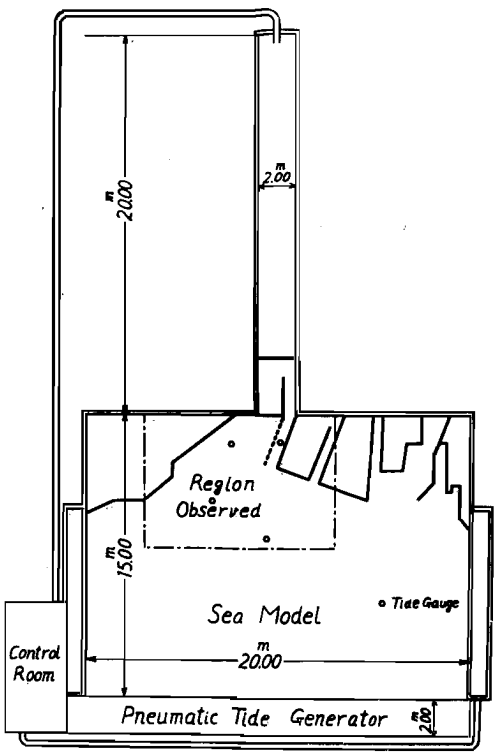

Fig. 8. Model of Hiroshima Bay.

Since the most important purpose of this experiment was to seek the model distortion which would satisfy the condition of dynamical similitude as stated before, the experiment was carried out for three cases of distortion, that is, $x_r/h_r=8$, 4, and 2. Therefore the vertical scale h_r was 62.5, 125, and 250 respectively. The time scale t_r was given by the equation (8) as 63.3, 44.7, and 31.6 respectively. Since the observed current might be regarded as semidiurnal, the corresponding periods of tide in the model were taken as 11.8, 16.7, and 23.6 min, respectively.

The standard tidal range in the prototype was assumed as 2.5 m, so that it was reduced in accordance with the value of h_r in the model. Dimensions of the model are shown in Table 2. Examples of tidal curves in the model

Table 2. Dimensions in the bay model experiment.

Distrotion of model x_r/h_r	Vertical Scale h_r	Water Depth h	Amplitude H	Time Scale t_r	Period T	Velocity Scale u_r	Velocity u
Prototype		500 cm	250 cm		12^h25^m		10 cm/sec
1	500	1	0.5	22.4	33′12″	22.4	0.446
2	250	2	1.0	31.6	23′36″	15.8	0.633
4	125	4	2.0	44.7	16′40″	11.2	0.893
8	62.5	8	4.0	63.3	11′46″	7.9	1.266

In which the horizontal scale $x_r=500$.

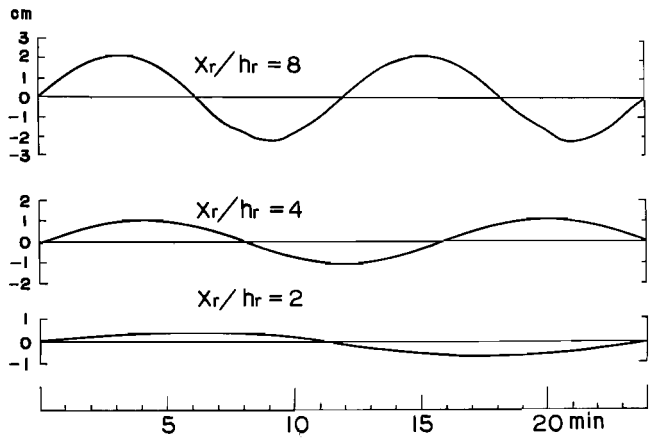

Fig. 9. Tidal curve in the model of Hiroshima Bay.

are shown in Fig. 9. which were measured at the station nearest to the tide generator shown in Fig. 8. The coast in the model was made with concrete blocks, and the bottom topography of sea and estuary was formed by sand. The flow was entirely within the laminar regime, and the bottom material did not move at all.

As shown in Photo. 9, over the model many white threads were rigged to form the reference coordinates and a network of a number of 1 square m covered the whole surface. The velocity and line of flow at each point were measured by photographing every minute or every half minute many floats from the top of a tower 3 m high. The water levels at four points shown in Fig. 8 were recorded by the level meter using the pick up of type A (Fig. 2). The direction of progression of tidal wave was decided by refering to the

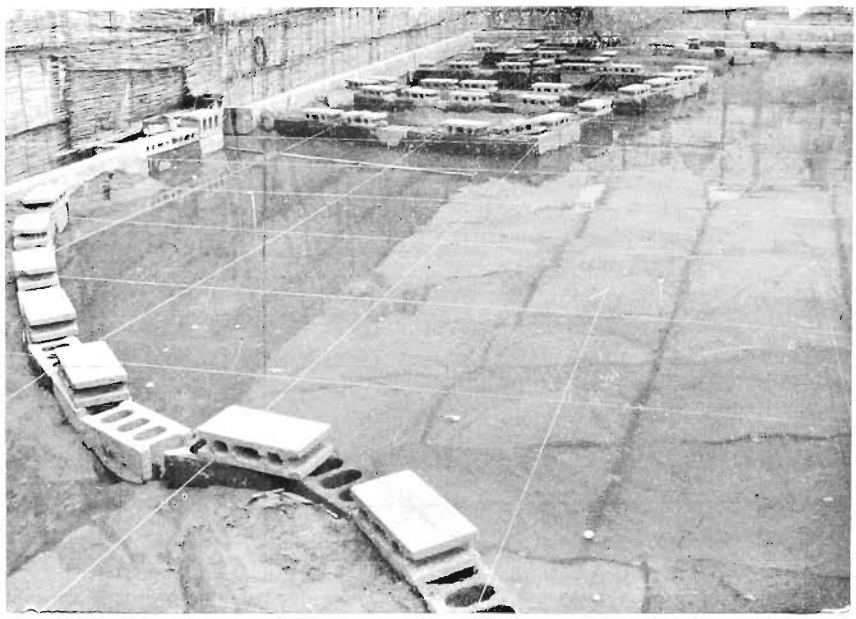

Photo. 9. Model of Hiroshima Bay.

prototype. The rate of fresh water flow in Fukushima River was neglected because it was very weak during the field observation.

During the preliminary experiment, it was found that the effect of the wind was considerable, hence the basin was covered temporarily with a polyethylene sheet (Photo. 8). However, as it was impossible to protect it completely from the wind, the experiments were carried out on calm days.

3. Results of experiment

The results of the experiments are shown in Fig. 10~15. In order to compare with Fig. 5 and 6, only the tidal current near the maximum velocity are shown in these figures, and the numerals show the value calculated by the equation (5) or (6) as the prototype. Fig. 10 and 11 show the results for the case in which $x_r/h_r=8$, Fig. 12 and 13 for $x_r/h_r=4$, and Fig. 14 and 15 for $x_r/h_r=2$. In these figures it is found that in the case in which $x_r/h_r=8$ the velocity is weaker than in the prototype and it increases from the offing toward the mouth of river. In the case in which $x_r/h_r=4$, the velocity is also lesser than in the prototype and almost uniform everywhere. However, in the case in which $x_r/h_r=2$, the velocity agrees well with the

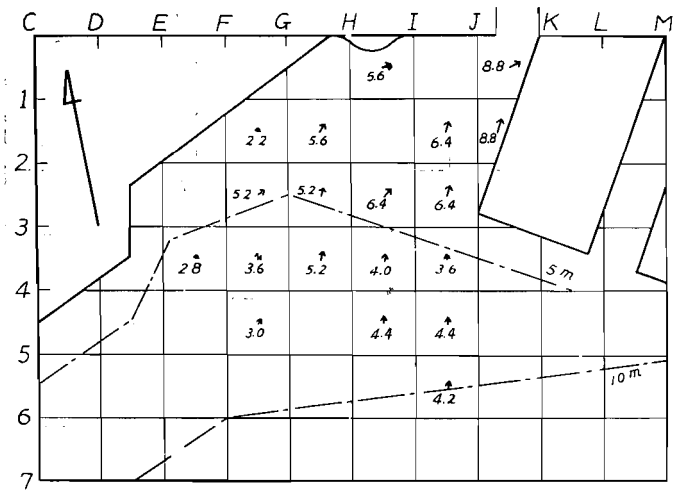

Fig. 10. Pattern of the maximum flood current. Model, $x_r/h_r=8$.

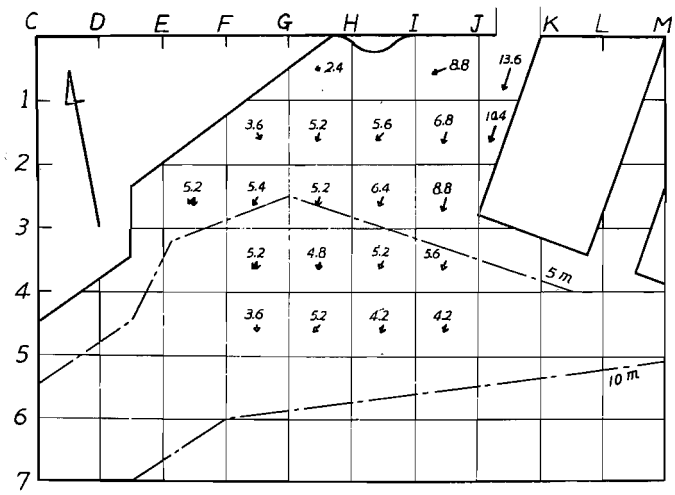

Fig. 11. Pattern of the maximum ebb current. Model, $x_r/h_r=8$.

prototype and the decrease of velocity is noticed near the contour-line of 5 m. Furthermore, near the left bank of Fukushima River, a counter-current is found at flood tide as in the prototype, and in the north western part, an eddy motion at ebb tide. So, in this case, it may be said that the tidal current in the model is similar to that in the prototype not only qualitatively but also quantitatively. Considering the error of the observation and the

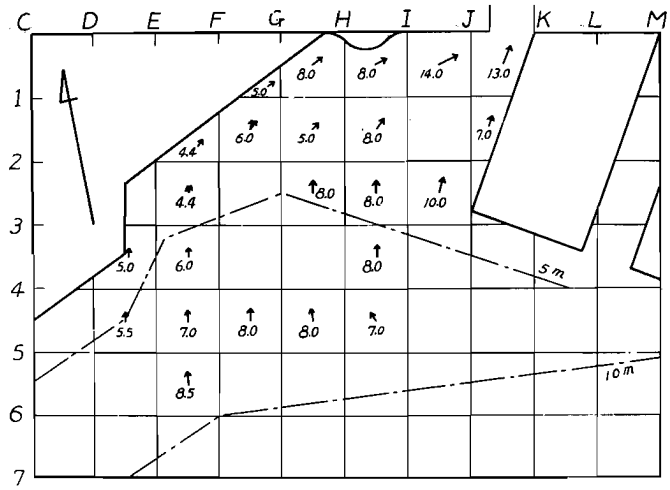

Fig. 12. Pattern of the maximum flood current. Model, $x_r/h_r=4$.

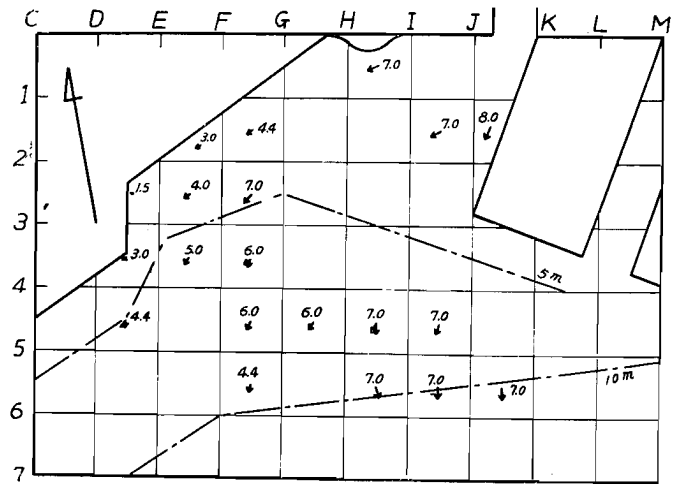

Fig. 13. Pattern of the maximum ebb current. Model, $x_r/h_r=4$.

experiment, the similarity between the prototype and the model is quite good.

As mentioned above, there is a plan to construct a training dyke of 1.5 km in length in the estuary at the right bank of Fukushima River. It will be interesting to note how the tidal current in the neighborhood of this will be changed after the completion of this plan. After the similitude was verifi-

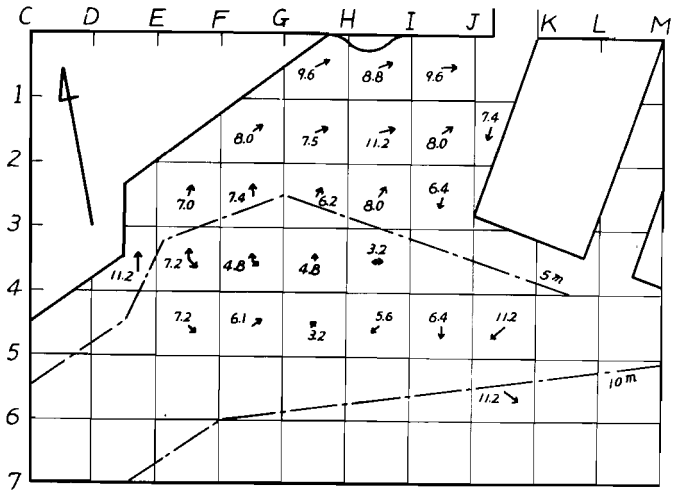

Fig. 14. Pattern of the maximum flood current. Model, $x_r/h_r=2$.

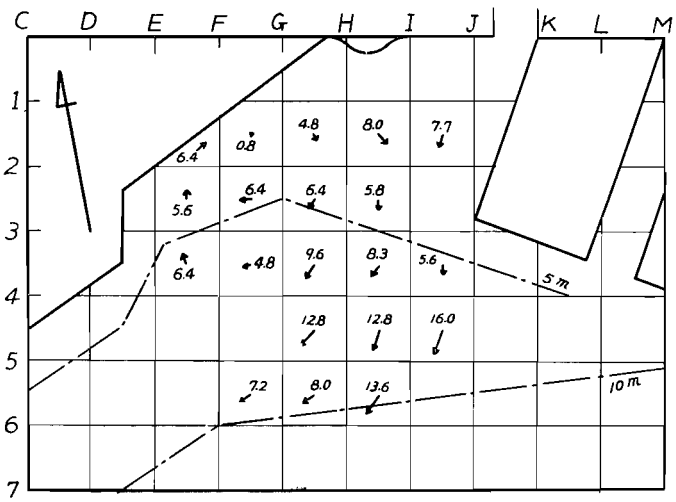

Fig. 15. Pattern of the maximum ebb current. Model, $x_r/h_r=2$.

ed, the experiments were carried out under the same conditions in which the similitude was held, except that the dyke was constructed. The results of this experiment are shown in Fig. 16 and 17. According to these results, the velocity in the western area of the dyke is reduced to less than half of the previous one ; and especially near the dyke, the reduction is extreme. The influenced area seems to be of the square of the length of dyke.

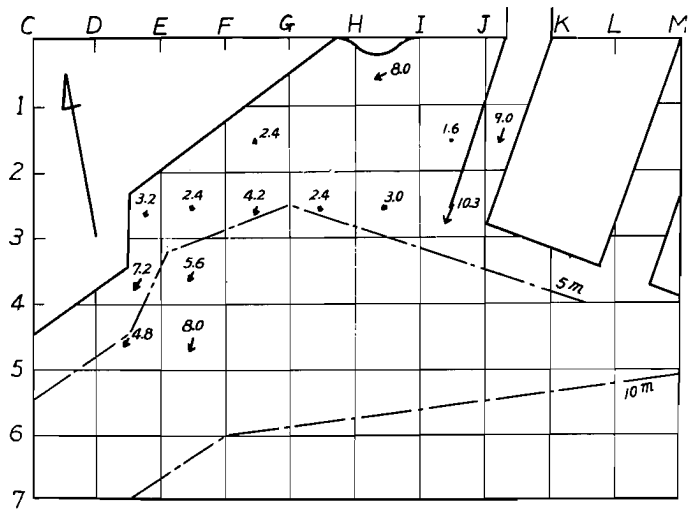

Fig. 16. Effect of the training dyke in the estuary of the Fukushima River Pattern of the maximum flood current. Model, $x_r/h_r=2$.

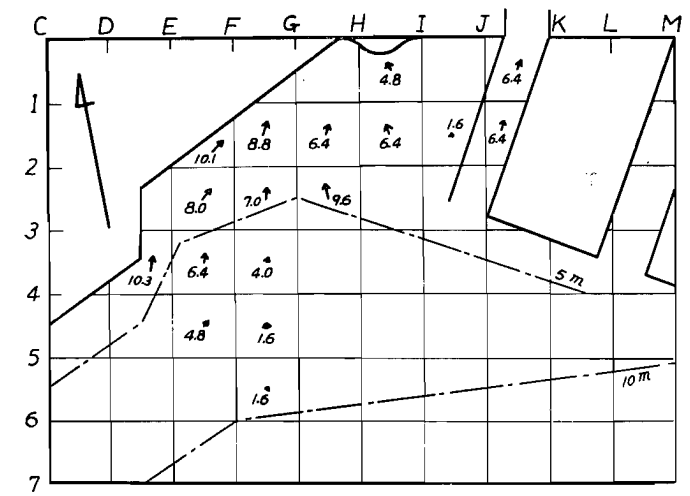

Fig. 17. Effect of the tranining dyke in the estuary of the Fukushima River. Pattern of the maximum ebb current. Model, $x_r/h_r=2$.

4. Consideration on similitude

From the results obtained above, the ratio of the drag coeffiicient may be decided as follows,

$$\frac{C_m}{C_p}=2\,. \tag{10}$$

The drag coefficient is generally a function of Reynolds number, and for laminar flow this functional relation is sufficiently expressed by Blasius' formula for skin friction,

$$C_m=\frac{1.328}{\sqrt{Re_m}}, \quad \text{for} \quad Re_m<5\times10^5 \tag{11}$$

Although this formula holds good in the case of a steady motion, it is assumed tentatively that it holds also good for the vertically mean velocity of the tidal current when Reynolds number is expressed by the maximum velocity of the tidal current U, and the length of the tidal excursion L, because the tidal current in the model changes very slowly. Such Reynolds number calculated from the results of the experiments are shown in Table 3, each of them is smaller than 5×10^5 so that the flow was laminar. Therefore, the equation (11) may be applied in these cases and the calculated values of C_m are shown in Table 4.

Table 3. Obtained Reynolds number in the bay model.

x_r/h_r :	2	4	8
Re :	1.79×10^4	1.28×10^4	1.38×10^4

Table 4. Frictional coefficient of the bay model.

x_r/h_r :	2	4	8
Cm :	0.99×10^{-2}	1.17×10^{-2}	1.13×10^{-2}

by equation (11)

On the drag coefficient in the prototype, G. I. Taylor (1918) proposed $k=2\times10^{-3}$ when the frictional force was assumed as $F=k\rho U^2$ by analogy to the river flow and the wind blowing over the surface of the earth, and applying the mean velocity of the tidal current in the Irish Sea, he obtained good results by finding that the calculated value of energy dissipation by friction coincided with the energy inflows of the tidal current from the both ends of this area. Jeffreys (1920) applied this value to the other oceans and made assumption of the energy dissipation of tidal motion throughout the earth. Grace (1929, 1936, 1937) obtained $k=1.4\sim4.1\times10^{-3}$ and $k=2.4\sim21.3\times10^{-3}$ from the observations in Bristol Channel and English Channel. K. F. Bowden and L. A. Fairbairn obtained $k=1.42\sim2.04\times10^{-3}$ (average $1.8\times$

10^{-3}) from the observation in Red Wharf Bay, and K. F. Bowden obtained $k=1.1\sim2.8\times10^{-3}$ (average 2×10^{-3}) by using electro-magnetic current meter in the same place. Although these values are scattered in a comparatively wide range, they can be regarded as $2.0\sim2.5\times10^{-3}$. This value of k is equivalent to $4\sim5\times10^{-3}$ for C_D.

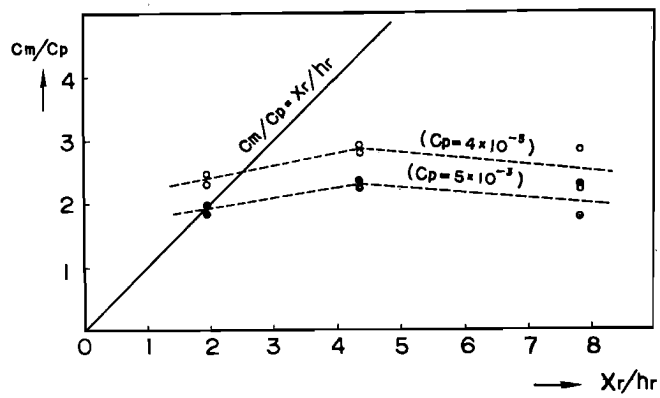

Fig. 18. Relation between the model distortion and the ratio of frictional coefficients (Observed and theoretical).

Now, assuming that $C_D=4\times10^{-3}$ and $C_D=5\times10^{-3}$ and the values in Table 4 for C_m, the relation between C_m/C_D and x_r/h_r is shown in Fig. 18. In this figure a straight line indicates the relation $C_m/C_D=x_r/h_r$. Any point on this line satisfies the theoretically required condition. From this result it may be admitted $C_D=5\times10^{-3}$ and $x_r/h_r=2$, and the formula (11) are available for tidal motion in the model.

When the similitude between the prototype and the model hold good, the relation of the velocity, $u_r=x_r/t_r$, must be established and further, equation (8) is substantial. Substituting these relations for Reynolds number of the prototype $Re_p(UL/\nu)$, we obtain the next equation.

$$Re_m=\frac{Re_p}{x_r h_r^{1/2}} \tag{12}$$

This equation shows the relation that is satisfied by both Reynolds numbers in the prototype and the model. The mean value of Re_p calculated from the result of the observation in the prototype is $Re_p=1.4\times10^8$ ($U=9.7$ cm/sec, $L=1.4\times10^6$). The values of Re_m for various values of x_r/h_r which were calculated from equation (12) are shown in Table 5, when $x_r=500$.

Table 5. Required Reynolds number in the model.

x_r/h_r :	2	4	8
Re_m	1.7×10^4	2.5×10^4	3.4×10^4

by equation (12)

The calculated value of Reynolds number shown in this figure coincides with the experimental value when $x_r/h_r=2$, implying that when the similitude holds good the equation (12) is substantial. If we substitute Re_m of the equation (12) for the equation (11) the following relation is obtained,

$$h_r^{5/4}=\frac{C_D}{1.328}Re_p^{1/2}x_r^{1/2} \tag{13}$$

The formula provides a general relation between the horizontal scale x_r and the vertical scale h_r in the model which is dynamically similar to the prototype. According to this formula, the realization of similarity in the case in which $x_r/h_r=2$ is simply due to the adopted value of the horizontal scale, that is $x_r=500$. A different value of x_r gives a different value of h_r, for example, $h_r=190$ when $x_r=250$. A larger h_r correspond with a larger x_r, then the water depth in the model becomes very shallow rendering the experiment difficult to do. On the contrary, a smaller h_r corresponds with a smaller x_r, then the model becomes large and a doubt arises as to whether the tidal current in the model will pass through the laminar regime, and further, it becomes difficult to protect the model from the wind. It is important to consider these points when a model experiment is projected.

3. Experiment for inlet model

1. Prototype

In this case, the area involving Sakai Channel, Nakaumi and a part of Miho Bay, which lie near the border between Tottori Prefecture and Shimane Prefecture, was chosen as the prototype. This is shown in Fig. 19. Nakaumi is 102 km² in area and 4.6 m in mean water depth. From the north west part of it, Sakai Channel, 7.5 km in length, 200～500 m in breath and 4.5～8 m in depth, runs eastward emptying into Miho Bay, Japan Sea.

For the past few years, various investigations were done in the prototype. For example, with respect to the water level, eleven tide stations were es-

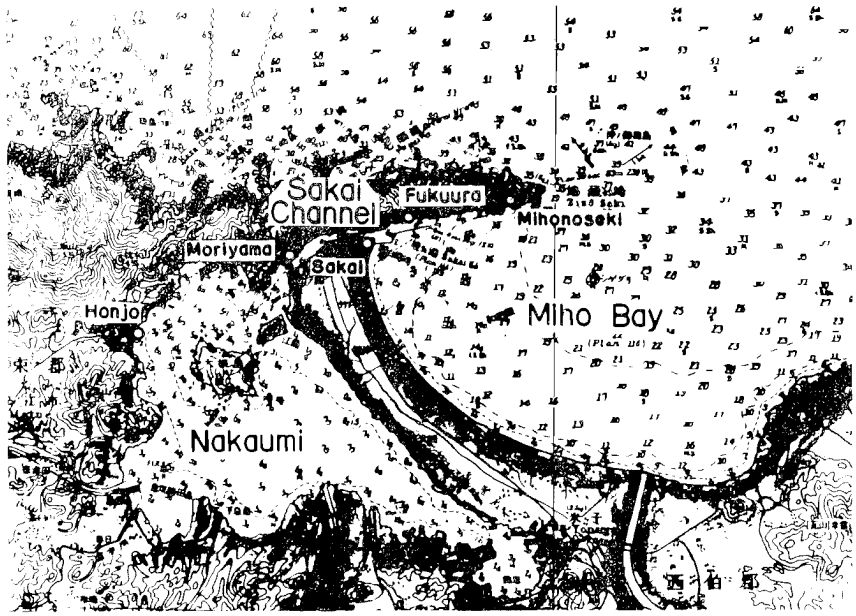

Fig. 19. Prototype of the inlet model.

tablished in this area and the daily tidal curves have been obtained. According to these, the monthly mean sea levels are lowest in February and March, and highest in July and August, and the difference between highest and lowest is 35~40 cm, which is almost constant everywhere. The tidal constituents are that $K_1=3.7$ cm, $O_1=3.5$ cm, $S_2=3.5$ cm, and $M_2=1.1$ cm at Sakai Tide Station. These values at each station are shown in Fig. 20 in the form of the ratio to Mihonoseki. As shown in this figure, the amplitudes of both the diurnal tide and semidiurnal tide decrease in the inner part of the channel, and they are reduced to 70% and 50% respectively at Moriyama. Besides the tide, a number

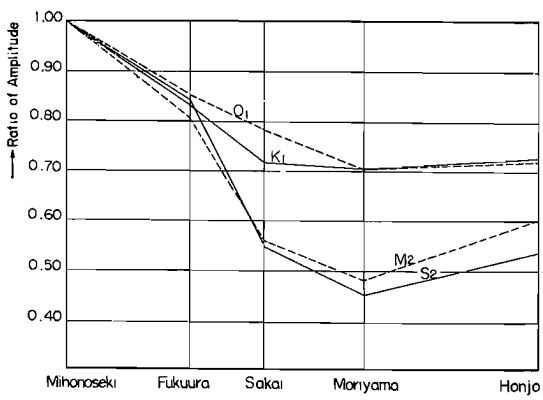

Fig. 20. Ratios of the amplitudes of the tidal constituents in prototype.

of rather long-period oscillations in comparison with the wind wave and swell are observed at every station, and their period is distributed in a wide range. Among these oscillations, there are many common oscillations at each station. The frequency distribution of these oscillations at Mihonoseki in 1957 is shown in Fig. 21. In this figure the oscillation of period of 75 minutes appears most frequently. From the data taken during the summer when the mean sea level is higher, we analysed a common oscillation of period of 130 minutes which are evident at each station in Sakai Channel. As the result of this analysis it was clarified that the amplitude of this oscillation at Moriyama was reduced to about 30% lower than that at Fukuura, and that in Nakaumi could not be identified.

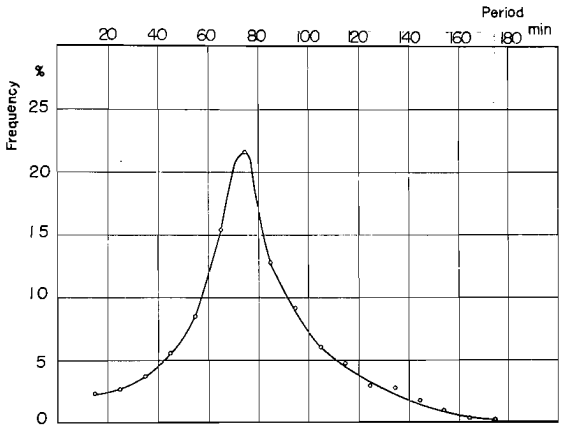

Fig. 21. Frequency distribution of long period's oscillation at Mihonoseki.

Chilean Tsunami, which attacked our country in May 1960, propagated in this area. Although these data were not obtained before the experiment was started, these were analyzed because they were important data in examining the similitude. The results are shown in Fig. 22 and 23. Fig. 22 shows the relation between the amplitudes and the period at each station, and Fig. 23 shows the ratio of amplitude,

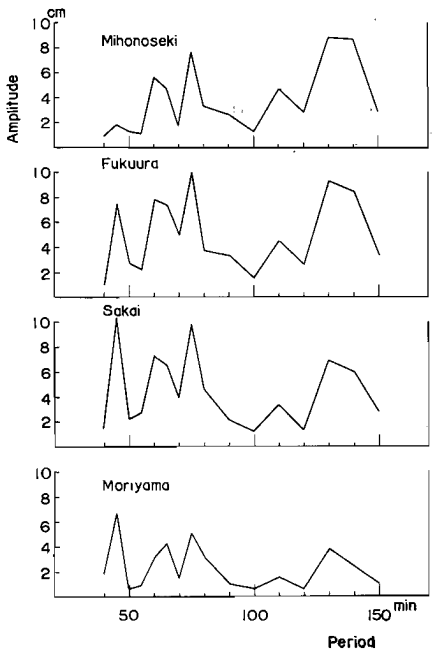

Fig. 22. Periodgram of Chilean Tsunami in Sakai Channel.

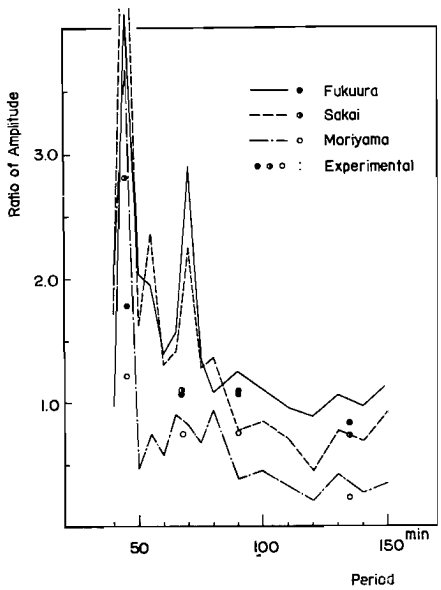

Fig. 23. Ratio of the amplitudes of Chilean Tsunami in Sakai Channel.

that is, the amplification factor, at each station for Mihonoseki. The oscillations of 60, 75, and 130 minutes dominated at Mihonoseki, while those of 20~40 minutes dominated in the coast of Pacific Ocean. In this case, 75 minutes' oscillation, which gives the maximum value in frequency distribution shown in Fig. 21, and 130 minutes' oscillation, which appeared in July 1957, dominated again. They may probably be characteristic periods of Miho Bay or more broad areas. The reason why 45 minutes' oscillation dominated in the channel is considered to be because this period coincided with the characteristic period of the channel itself, and that a resonance effect occured. The characteristic period of a channel opened at both ends is given by $T_0=2L/\sqrt{gh}$ when the friction is neglected. In the case of Sakai Channel, $L=7.5$ km and $h=5.7$ m (average value), T_0 is about 33 minutes. The real characteristic period of Sakai Channel, 45 minutes, is a little longer than this period. It is considered that the energy dissipation at the ends of the channel and the complexity of the form elongate the characteristic period.

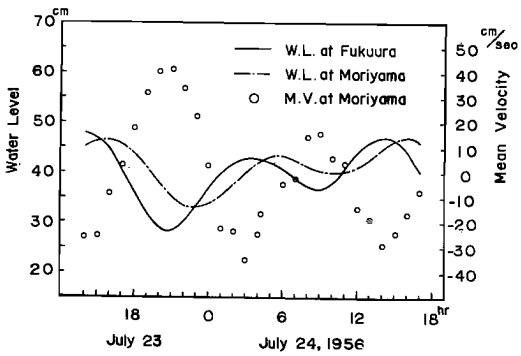

Fig. 24. Velocity of flow at Moriyama and water levels at Fukuura and Moriyama. Prototype July 23 and 24, 1956.

On the velocity of flow, the field observations were made eleven times at Moriyama from September 1954 to July 1957. One of the results of observations is shown in Fig. 24. From

the results, the relation between the ratio of the amplitude at Moriyama and the amplitude at Mihonoseki, and the relation between the velocity of flow at Moriyama and the amplitude at Mihonoseki are shown in Fig. 25. In this figure it seems that the maximum mean velocity at Moriyama is proportional to 2/3 power of the amplitude at Mihonoseki. The upper figure shows that the ratio of the amplitude is constant within this range of the amplitude.

The discharge by inflow from Nakaumi was neglected since it was weak during the field observation.

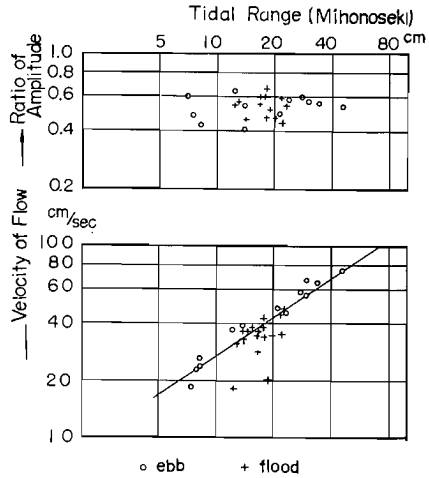

Fig. 25. Effects of the amplitude on the ratio of amplitudes of the semi-diurnal tide and on the maximum mean velocity at Moriyama. Prototype.

2. Procedure

In order to decide the distortion of the model in which the similitude holds good, the preliminary experiment was at first carried out with a simplified model. Then the precise experiment was done with an accurate model, the distortion of which was that decided by the preliminary experiment. After the similitude was examined both by comparing with the prototype and by the theoretical consideration, the oscillation response of the model was examined under several channel configuration.

i) Preliminary experiment

The horizontal scale was decided as $x_r = 500$. As shown in Fig. 26, the model involved a part of Miho Bay, the whole of Sakai Channel, and a part of Nakaumi. In the preliminary experiment, the area of Nakaumi in the model was 48% of the required one (Photo. 10). The cross section of the channel was rectangular and the bottom was horizontal for the convenience of the experiments to seek the suitable model distortion. Side walls of the model were constructed with concrete blocks, and the bottom was made of mortar and finished by brush. During the experiments the channel was covered by vinyl plates for protection from the wind.

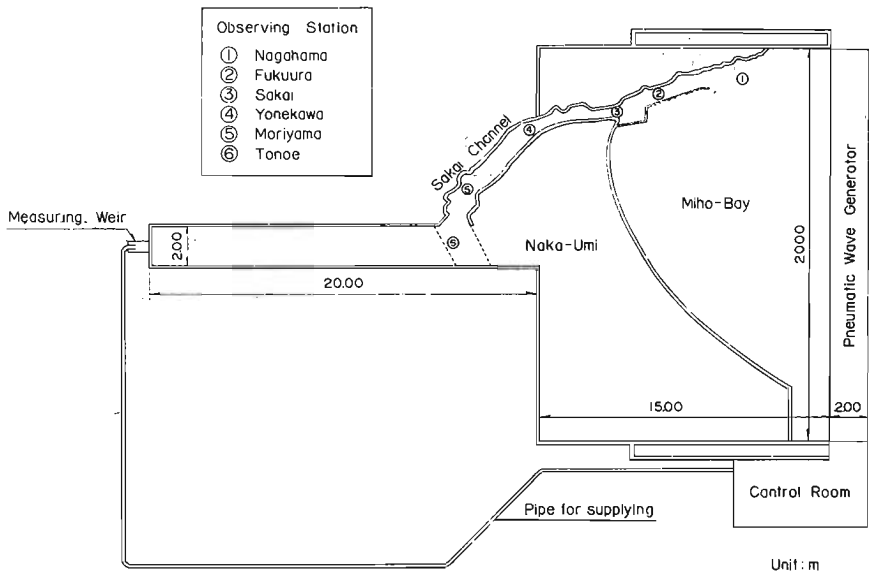

Fig. 26. Model of Sakai Channel for the preliminary experiment.

Photo. 10. Model of Sakai Channel for the preliminary experiment.

The water levels at ①～⑥ in Fig. 26 were measured by the level meter, using the pick up type B (Fig. 2). The velocity of flow at the water surface was measured in the neighborhood of ⑤ by tracing the floats.

Since the area of Nakaumi was not sufficient, the strict similitude was not expected, so that the suitable model distortion, in which the mode of damping of the semidiurnal tide and 130 minutes' oscillation were similar to the prototype, was sought by changing the vertical scale with a constant horizontal scale. That is, the horizontal scale was always fixed as $x_r=500$, while the vertical scale was chosen for five distortions, $x_r/h_r=2$, 4, 6, 8, and 16. Considering Froude number, the hydraulic factors in the model and the prototype are shown in Table 6.

Table 6. Dimensions in the inlet model.

Distortion of Model x_r/h_r	Vertical Scale h_r	Water Depth h	Amplitude H	Time Scale t_r	Period T		Velocity Scale U_r	Velocity u
Prototype		500 cm	20 cm		130 m	12h25m		40 cm/sec
1	500	1	0.04	22.4	5′48″	33′12″	22.4	1.79
2	250	2	0.08	31.6	4′07″	23′36″	15.8	2.53
4	125	4	0.16	44.7	2′55″	16′40″	11.2	3.57
6	83.4	6	0.24	54.7	2′23″	13′38″	9.13	4.38
8	62.5	8	0.32	63.3	2′03″	11′46″	7.90	5.07
16	31.25	16	0.64	89.4	1′27″	8′20″	5.59	7.15

in which the horizontal scale $x_r=500$

When $x_r/h_r=1$, the water depth in the model channel is only as small as 1 cm, and therefore it is difficult to carry out the experiment with small error considering the accuracy in constructing the bottom. From this reason, this case was omitted, and the experiment was carried out in the other distortions. Since the amplitudes of the tide and the other long-periods oscillations are about 20 cm, and scarcely exceed 40 cm, those in the model would be reduced to only several mm, and it is also too difficult to carry out the experiment. So, the experiment for the oscillation having the amplitude of 1 cm mainly were carried out.

The experiment to examine the behavior of the semi-diurnal tide and 130 minutes' oscillation was first carried out in each distortion by providing the sinusoidal waves to Miho Bay.

Next, the frictional coefficient of the model channel was sought in steady flow by using the river flow feeder and point-gages. The reason why point-gages were used was that the experimental error by the shift of zero point which was inevitable in the electric measurement would be reduced by using them.

Since, by the foregoing experiment, it became to be clear that the mode of damping of the semidiurnal tide in the channel was similar to the prototype when the distortion was 4, the behaviors of the oscillations of various periods were examined. Ten kinds of periods from 1 to 32 minutes were provided for this purpose.

Then the behaviors of those in the channel closed as shown in broken lines in Fig. 26 were examined, and these were compared with preceding results. After this, the effect of the amplitude of semidiurnal tide and 130

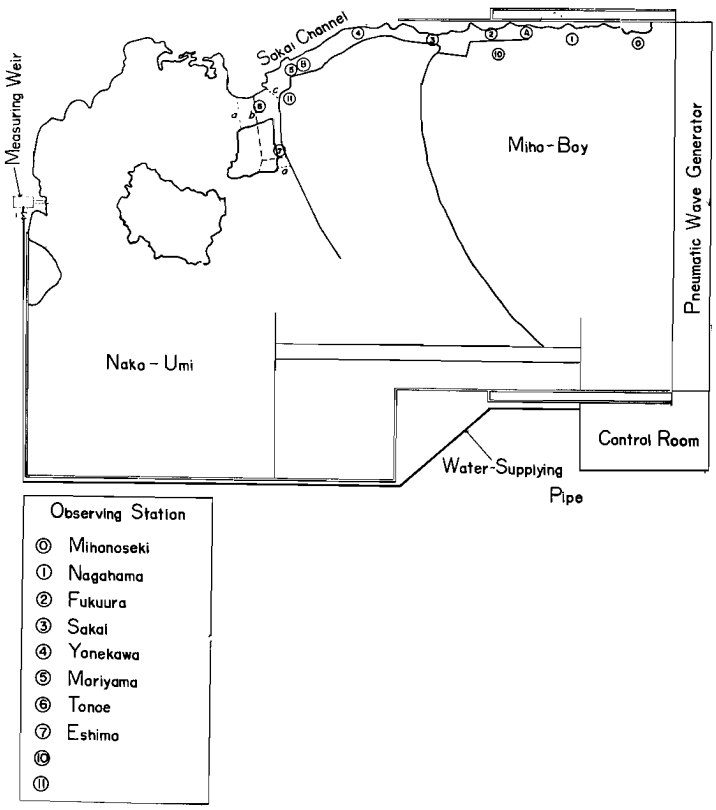

Fig. 27. Model of Sakai Channel for the precise experiment.

Photo. 11. Model of Sakai Channel for the precise experiment.

minutes' oscillations were examined.

ii) Precise experiment

The model was constructed of the distortion 4, that is, $x_r=500$ and $h_r=125$, which were decided by the results of the preliminary experiment. As shown in Fig. 27 this model involved a part of Miho Bay, the whole of Sakai Channel, and Nakaumi. Although the form of Nakaumi was deformed a little,

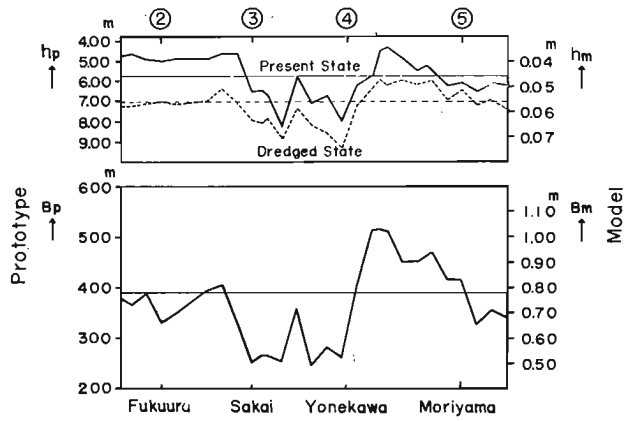

Fig. 28. Water depths and breadth of Sakai Channel in the prototype and the model.

its area was what was required by horizontal scale. The accurate model was also constructed with concrete blocks and mortar. The accurate bottom topography was made of the whole of Sakai Channel, parts of Miho Bay and Nakaumi. The breadth and the water depth of the channel in the prototype and the model are shown in Fig. 28. In this figure the full line shows the present state and the broken line after proposed dredging.

The method of measurement of the water levels were the same as before. The velocities of flow were measured at Ⓐ or Ⓑ in Fig. 27, by using the moment type current meter. The oscillations were provided by automatic control.

First, the frictional coefficient was sought, then the similitude was examined. This is the experiment used to seek the conditions in which the similitude obtains. The oscillations of various amplitudes from 0.3 to 2.0 cm were provided for practical purposes, and the velocities of flow and amplitudes were measured at the station ⑤, which were compared with the prototype.

Then the frequency response of the model of the present state was sought by examining the behavior of the oscillations of various periods from 1 to 32 minutes. These periods correspond with those from 45 minutes to 25 hours in the prototype.

After that, experiments of the same kind were carried out in some modified configurations. The configuration of the model was such that the channel was closed at "a" or "b" or "c" in Fig. 27 and the bottom of it was as the present state or the dredged state in the prototype. The area between "a" and "b" equaled that between "c" and "b" In these experiments the oscillations of the period which was longer than 12 minutes were omitted since the oscillations of longer periods changed little when the channel was closed and they were scarsely interesting.

Finally, the effect of the water depth on the frequency response was examined in a straight uniform channel with a small reservoir, the area of which was equal to that when the channel was closed at "a" or "c"

3. Results of experiment

i) Preliminary experiment

a) The amplitudes of the semidiurnal tide at each station in each distortion from 2 to 16 are shown in Fig. 29 as the ratio to that at ②, for convenience to compare with the prototype because the model did not involve Mihonoseki. From this figure it is found that the smaller the distortion be-

comes, the more the damping. This means probably that since the shallower water corresponds to the slighter distortion, the effect of the friction in the channel becomes greater. The mark ○ shows the value of the prototype. Excepting the value at ③, the state of damping seems to be similar to the prototype in the case of distortion 4. Fig. 30 shows the state for the 130 minutes' oscillation. From this figure it is found that the state in each case is almost the same. This may suggest that the effect of the friction in the channel on these oscillations of shorter period is very slight.

Then the effect of the amplitude on the state of damping was examined in the case of distortion 4 for both the semidiurnal tide and the 130 minutes' oscillation. Fig. 31 shows the result for the semidiurnal tide, in which the numeral shows the amplitude at ②. From this

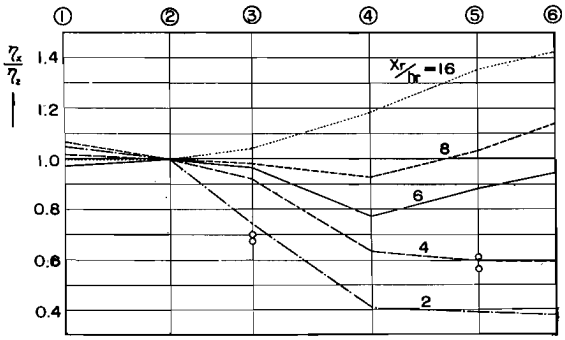

Fig. 29. Effect of the model distortion on the ratio of the amplitudes of the semidiurnal tide. Model, with the large reservoir. Mark ○ shows the value of the prototype.

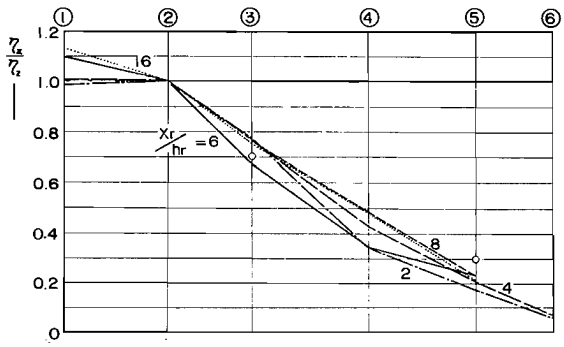

Fig. 30. Effect of the model distortion on the ratio of the amplitudes of the 130 minutes' oscillation. Model, with the large reservoir. Mark ○ shows the value of the prototype.

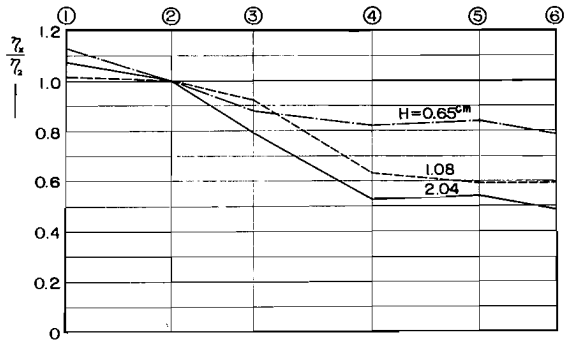

Fig. 31. Effect of the amplitude on the ratio of the amplitudes of the semidiurnal tide. Model, with the large reservoir.

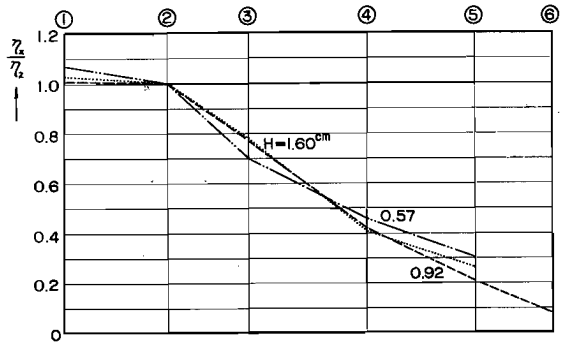

Fig. 32. Effect of the amplitude on the ratio of the amplitudes of the 130 minutes' oscillation. Model, with the large reservoir.

it is found that in the case of the larger amplitude, the larger damping appears. Fig. 32 shows that for the 130 minutes' oscillation. It is found that the state is almost the same as Fig. 30.

From these, it was clarified that the effect of the distortion was great on the oscillation of as long period as the semidiurnal tide but that was slight on the oscillation of as short period as 130 minutes' oscillation, and in the case of the distortion 4, the state of the semidiurnal tide was most similar to the prototype. However, it must be noted that it is correct only when the area of the reservoir is smaller and the amplitude of the oscillation has a particular value.

b) Frictional coefficient of the model

Since the frictional coefficient of the channel in the prototype was given in the form of Manning's roughness coefficient, that of the model was sought by measuring the gradient of the water surface in steady flow.

The flow was steady and the channel had the horizontal bottom and rectangular cross section. To simplify, assuming that the breadth of the channel is constant between successive stations, the following equation is derived from the equation of motion.

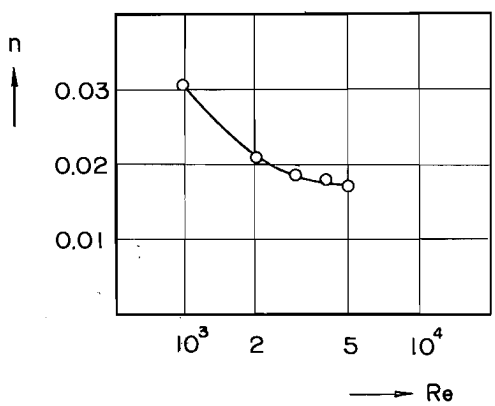

Fig. 33. Manning's roughness coefficient of the model channel in the preliminary experiment.

$$n^2 = \frac{R^{4/3}}{U^2} i_w \left(1 - \frac{U^2}{gh}\right) \qquad (14)$$

in which, n: Manning's roughness coefficient, and R: hydraulic radius. Fig. 33 shows the coefficient calculated by equation (14) in the case of the distortion 4.

c) Frequency response I

In the case in which the distortion was 4 and the amplitude was 1 cm, the frequency response, i.e., the behavior of the oscillations of ten different periods from 1 to 32 minutes was examined. The ratio of the amplitude, that is, the amplification factor, at each station referred to ② is shown in Fig. 34.

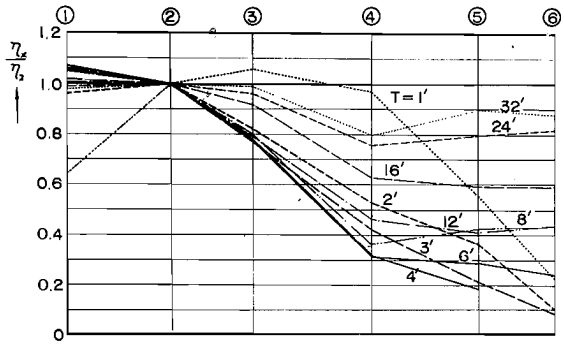

Fig. 34. Effect of the period on the ratio of the amplitudes of the oscillations of the same amplitude. Model with the large reservoir. Numeral shows the period in minutes.

From this figure it becomes clear that, except for 1 minute, as the period becomes longer, the ratios of amplitudes at each station become gradually lower till the minimum about 4 minutes, and then the ratios become high again with increase in the period. To understand this fact more easily, Fig. 35 is shown. The abscissa shows the period in minutes, and the ordinate shows the ratio of the amplitude as the above figure. Each curve in this figure shows the ratio at each station respectively. This figure indicates that the values of the ratio become minimum when the period lies between 3 and 6 minutes. The reason why the curve at ① shows the opposite form is that the ratio is refered to ②, and ① is located on the opposite side of the other stations.

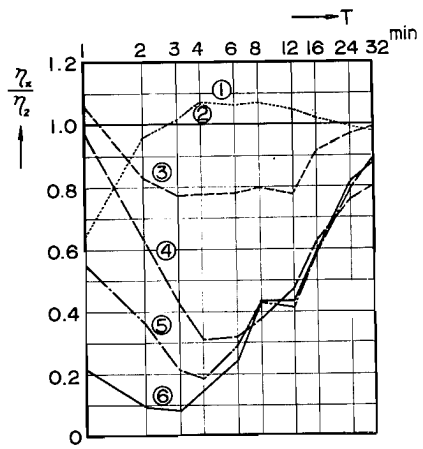

Fig. 35. Experimental frequency response. Model with the large reservoir. Number shows the observing location.

The results of the current measurement for the semidiurnal tide and the 130 minutes' oscillation are shown in Fig. 36.

d) Frequency response II

This series of experiments was carried out in the channel closed near ⑥ as shown by broken lines in Fig. 26. The results are shown in Fig. 37 and

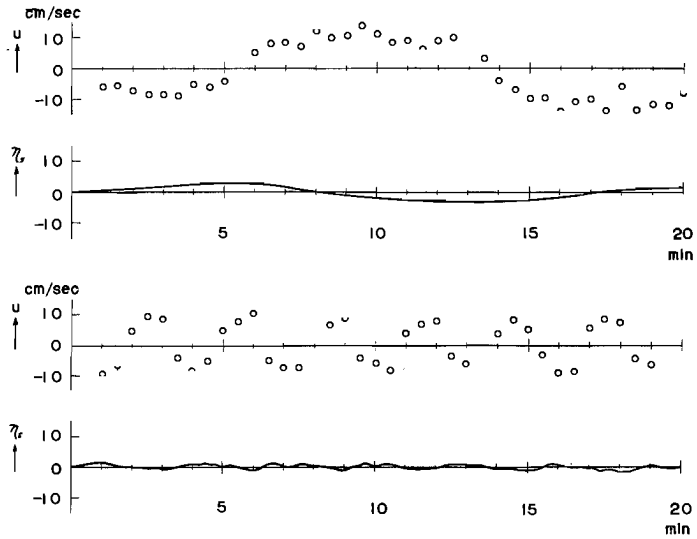

Fig. 36. Velocity of flow u at Ⓑ and water levels η_6 at ⑤ of the semidiurnal tide (top) and the 130 minutes' oscillation (bottom). Model with large reservoir.

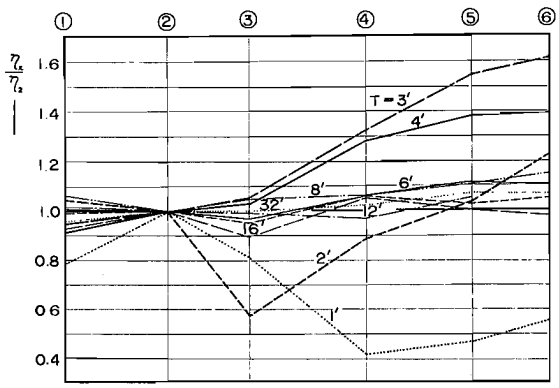

Fig. 37. Effect of the period on the ratio of the amplitudes of the oscillations of the same amplitude. Model with the small reservoir. Numerals show the period in minutes.

38. Fig. 37 corresponds to Fig. 34 in the preceding article. From this it becomes clear that the amplitudes of the oscillations of over 2 minutes do not decrease, but on the contrary increase. Fig. 38 corresponds to Fig. 35. This shows that each curve has the maximum value when the period is 3 minutes, and each curve gradually approaches unity when the period becomes

longer.

Then the effect of the amplitude of the semidiurnal tide and the 130 minutes' oscillation were again examined. The results are shown in Fig. 39 for the semidiurnal tide and in Fig. 40 for the 130 minutes' oscillation. From these it is found that the ratios of the amplitudes in this case are much different from those of the preceding case, that is, the ratios of the amplitudes of the semidiurnal tide do not vary throughout the channel for any amplitude, on the other hand, those of the 130 minutes' oscillation of small amplitude become larger in the inner part of the channel

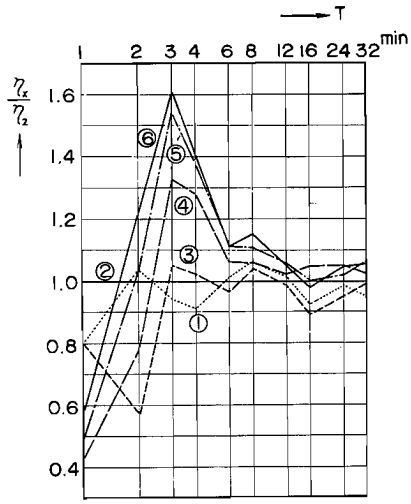

Fig. 38. Experimental frequency response in the channel with the small reservoir. Numbers show the observing location.

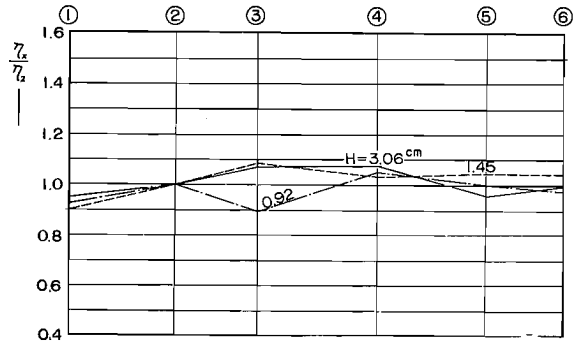

Fig. 39. Effect of the amplitude on the ratio of the amplitudes of the semidiurnal tide. Model with the small reservoir.

than those of large amplitude.

The velocities of flow and the water level of the semidiurnal tide and the 130 minutes' oscillation are shown in Fig. 41 as Fig. 36.

ii) Precies experiment

a) Frictional coefficient

Manning's roughness coefficient of the accurate model was obtained by the same method as in the preliminary experiment. These are shown in Fig.

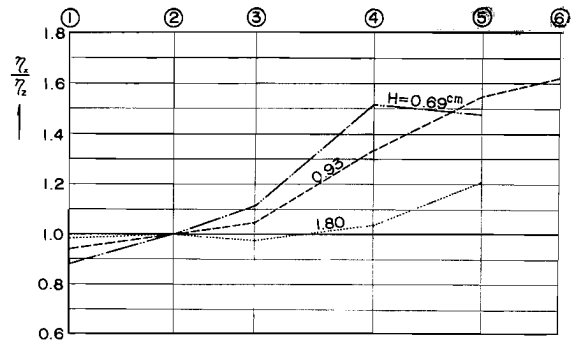

Fig. 40. Effect of the amplitude on the ratio of the amplitudes of 130 minutes' oscillation. Model with the small reservoir.

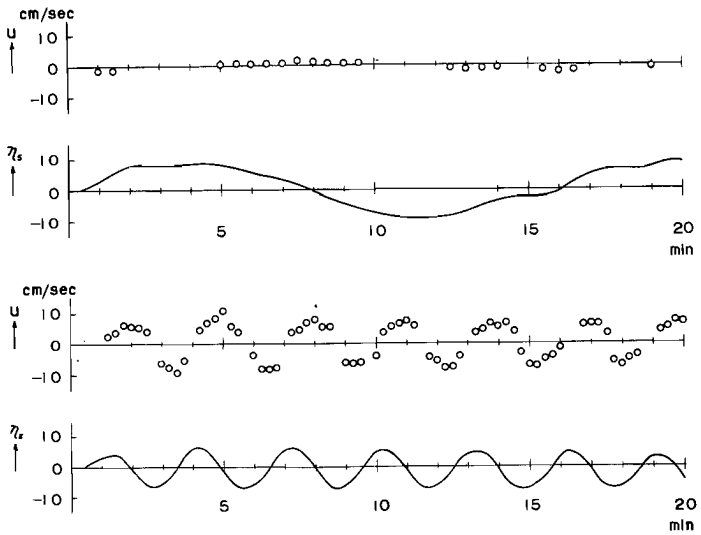

Fig. 41. Velocity of flow u at Ⓐ and water levels η_5 at ⑤ of semidiurnal tide (top) and 130 minutes' oscillation (bottom). Model with the small reservoir.

42. In this figure, the full line and the black circles refer to the present state, and the broken line and the white circles refer to the dredged state. From this figure, it is found that the roughness coefficient of the model channel changes in a comparatively wide range as in the preliminary experiment.

b) Experiment for similitude

The ratios of the amplitudes of the semidiurnal tide of various amplitudes are shown in Fig. 43. Eight different amplitudes were actually treated but

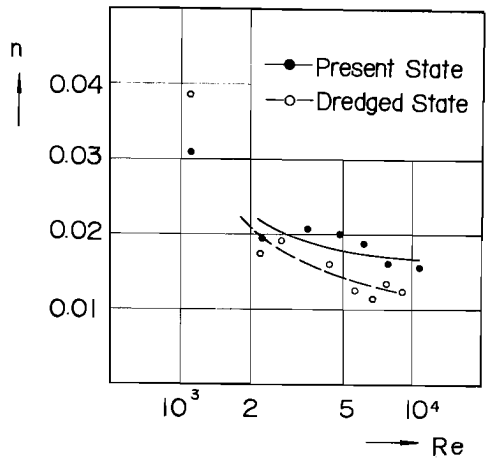

Fig. 42. Manning's roughness coefficient of the model channel in the precies experiment.

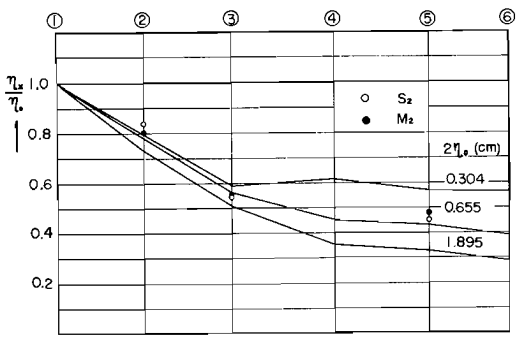

Fig. 43. Effect of the amplitude on the ratio of the amplitudes of the semidiurnal tide. Models Sakai Channel and Nakaumi are present state.

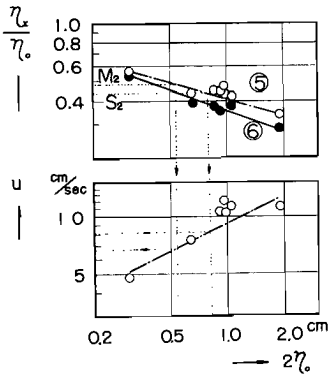

Fig. 44. Effects of the amplitude on the ratio of the amplitudes of semidiurnal tide and on the maximum mean velocity of flow at ⑤. Models Sakai Channel and Nakaumi are present state.

three representative cases are shown in the figure. The ratio is refered to ① and the numeral shows the amplitude at ①. This figure indicates that the mode of damping is different depending on the provided amplitude. This coincides with the result of the preliminary experiment. Comparing this figure with the prototype shown in Fig. 25, it is suggested that the similitude does not hold good about any amplitude.

The ratios of the amplitudes at ⑤, where the data of the prototype were obtained, and at ⑥, where it was thought to be the representative location

of the channel, are shown in Fig. 44 in the same expression as Fig. 25. Comparing this figure with the values of M_2 and S_2 in the prototype, it seems to be similar to the prototype when the amplitude is in the range from 0.5 to 0.8 cm.

c) Frequency response III

Since it became clear in the preliminary experiment that the system composed of both Sakai Channel and Nakaumi must be considered to make one oscillating system, the frequency response was examined in this precise experiment.

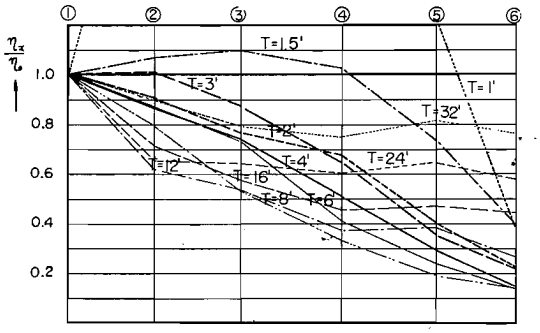

Fig. 45. Effect of the period on the ratio of the amplitudes. Models Sakai Channel and Nakaumi are pressent state.

The ratios of the amplitudes, refered to ①, in various periods at each station are shown in Fig. 45. In this figure, the curves of 1 and 1.5 minutes show the particular forms, and those of the other periods show the same forms as in the preliminary experiment qualitatively. However, the period which gives the minimum becomes longer than before. Fig. 46 shows the same result as Fig. 45 in the form as Fig. 35.

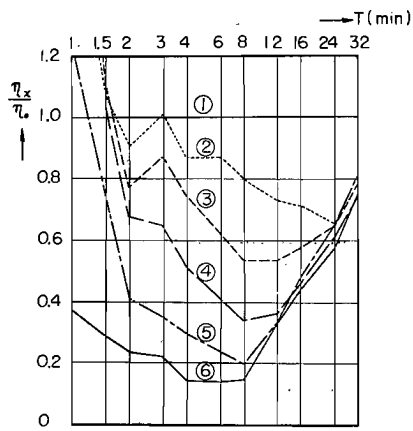

Fig. 46. Experimental frequency response. Models Sakai Channel and Nakaumi are present state.

d) Frequency response IV

This series of experiments was carried out in the channel closed at "a" in Fig. 27. The oscillations of several steps of the amplitude was examined for each period from 1 to 8 minutes.

Since it would be supposed by the results of the preliminary experiment and theoretical consideration that the oscillations of periods longer than 12 minutes change little their amplitude in this case, the experiment for these oscillations was omitted. This is applied also to the following articles.

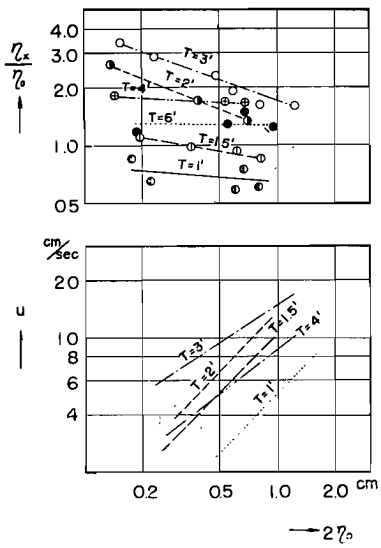

Fig. 47. Effects of the amplitude on the ratio of the amplitudes of the oscillations of various periods and on the maximum mean velocities. Model Sakai Channel is present state and Nakaumi has the area under planning.

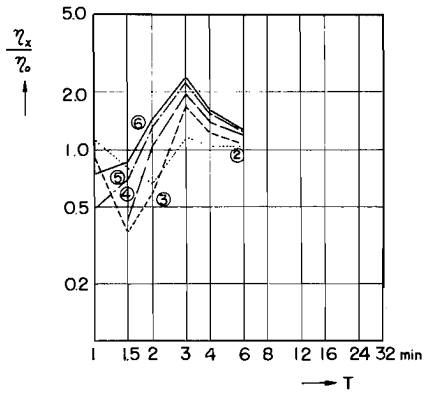

Fig. 48. Experimental frequency response. Model Sakai Channel is present state and Nakaumi has the area under planning.

The results are shown in Fig. 47, in which only the values at ⑥ are plotted to avoid the complexity. From this figure, only the values which satisfy the conditions of similitude are selected and shown in Fig. 48. This figure also shows the same nature as the preliminary experiment qualitatively. The characteristic period in this case is to be considered as 3 minutes.

e) Frequency response V

Then the channel closed at "c" in Fig. 27, just at the mouth of Nakaumi, and the same experiment as in the preceding article was carried out. The results are shown in Fig. 49. From this the selected values which satisfy the condition of the similitude are shown in Fig. 50. Since the station ⑥ was out of the domain concerned, the values show those at ⑤. Comparing with the results of the preceding experiment, it is found out that the period which provides the maximum becomes short and the maximum value becomes very large. The reason is considered to be that the characteristic period is shortened by the absence of the reservoir.

f) Frequency response VI

This series of experiments was carried out in the model with the channel of dredged state and closed at "b" in Fig. 27. The results are shown in

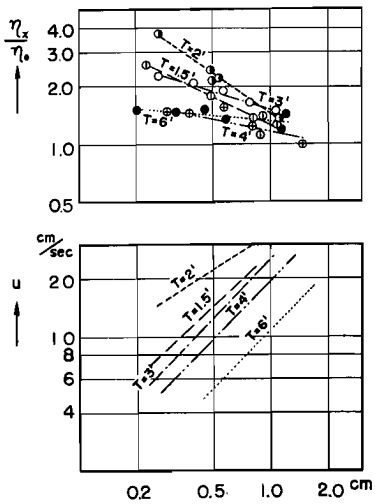

Fig. 49. Effects of the amplitude on the ratio of the amplitudes of the oscillations of various periods and on the maximum mean velocities. Model Sakai Channel is present state and Nakaumi has no area.

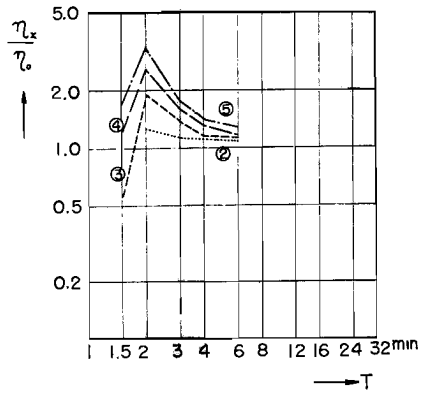

Fig. 50. Experimental frequency response. Model Sakai Channel is present state and Nakaumi has no area.

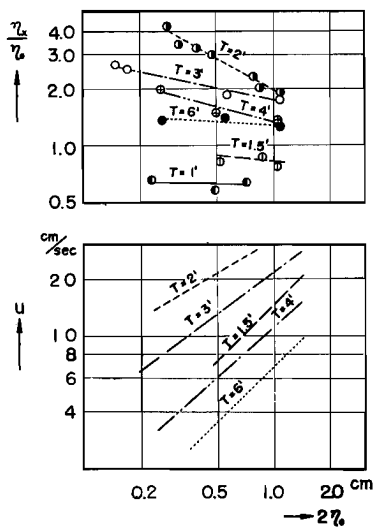

Fig. 51. Effects of the amplitude on the ratio of the amplitudes of the oscillation of various periods and on the maximum mean velocities. Model Sakai Channel has been dredged and Nakaumi has the area under planning.

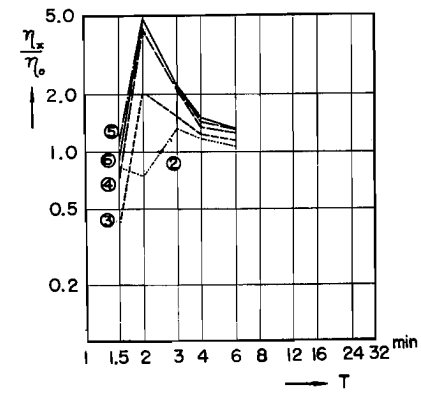

Fig. 52. Experimental frequency response. Model Sakai Channel has been dredged and Nakaumi has the area under planning.

Fig. 51 and 52.

Fig. 52 corresponds with Fig. 48. Comparing both figures, it is found that the curves are considerably different from each other. In this case the characteristic period may be shortened by the deepening of the channel.

g) Frequency response VII

To examine this fact, the additional series of experiments was carried out by using a straight uniform channel, in which the breadth and the mean water depth were the same as the accurate model of Sakai Channel, and a reservoir connected with the channel, the area of which was the same as between "a" and "c" or "b" and "c" in Fig. 27.

The results are shown in Fig. 53~56. Fig. 53 and 54 are the results in the case where the mean water depth was 4.5 cm, which corresponded with the present state, that is, with Fig. 47 and 48 respectively. Fig. 55 and 56 are those in the case of 6.0 cm, which corresponds with the dredged state, that is, with Fig. 49 and 50 respectively. Comparing these figures respectively, it is found that the forms are quite similar to each other respectively excepting the slight difference of the maximum values. From this, it is considered that the difference between Fig. 48 and 52 is explained only by the difference of the water depth.

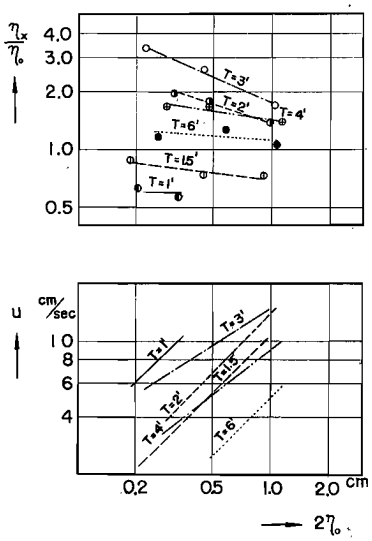

Fig. 53. Effect of the amplitude on the ratio of the amplitudes of the oscillations of various periods and on the maximum mean velocities. Model, straight channel with the reservoir of the area as large as planned, the water depth corresponding to the present state.

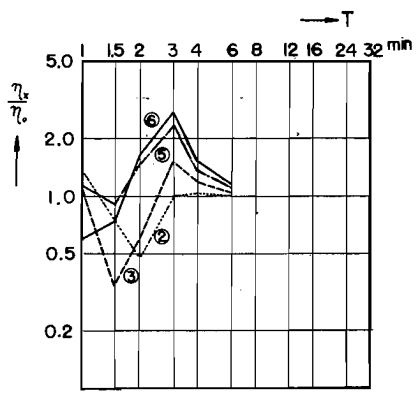

Fig. 54. Experimental frequency response. Model, straight channel with the reservoir of the area as large as planned, the water depth corresponding to the present state.

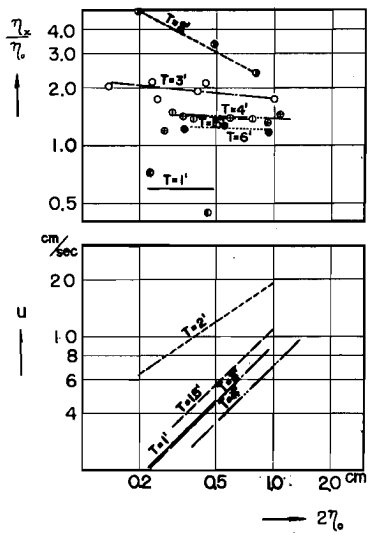

Fig. 55. Effect of the amplitude on the ratio of the amplitudes of the oscillations of various periods and on the maximum mean velocities. Model, straight channel with the reservoir of the area as large as planned, the water depth corresponding to the dredged state.

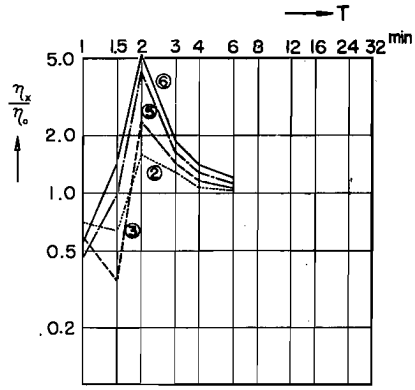

Fig. 56. Experimental frequency response, Model, straight channel with the reservoir of the area as large as planned, the water depth corresponding to the dredged state.

4. Consideration on similitude

As shown in Fig. 42, the roughness coefficient of the model changes with the Reynolds number, therefore, it is considered that the flow belongs to the transient regime. In such a case, we must be satisfied with the similitude that holds in some average value, taking the characteristic frictional coefficient of the model as C_m at some characteristic Reynolds number.

Now, in the case of Sakai Channel, Manning's roughness coefficient is given as the frictional coefficient of the prototype. Therefore, the equation (9) is written with the use of n as follows.

$$n_r = \frac{n_p}{n_m} = h_r^{2/3} x_r^{-1/2} \tag{15}$$

For the prototype, $n_p = 0.022$ was given. From this equation, $n_m = 0.0196$ is obtained when $x_r = 500$ and $h_r = 125$. This value of n_m is that which is required as the roughness coefficient of the model channel in which the dynamical similitude holds good. Then it is considered that, since, when this

value of n is realized the phenomena in the model are similar to the prototype, the Reynolds number which provides such value of n is defined as the characteristic Reynolds number.

In order to obtain such a Reynolds number, the oscillations of various amplitudes were examined. From this point of view, the reason why the damping state of semidiurnal tide in the model was similar to the values of M_2 and S_2 in the prototype when the amplitudes in the model were between 0.5 and 0.8 cm, is considered to be as follows: The velocity of flow in these cases was between 7 and 8 cm/sec, so that the Reynolds number was between 2.5×10^3 and 2.8×10^3. If the values in steady flow are correct in such a case, the roughness coefficient in this case is obtained being between 0.019 and 0.020 from Fig. 42, which is nearly equal to the characteristic roughness coefficient $n_m=0.0196$. In other words, the damping state resembled the prototype because the condition of the similitude on the frictional coefficient is satisfied when such amplitudes were provided. On the other hand, considering the velocity of flow, the mean velocity in the prototype is presumed that $u_p=90\sim120$ cm/sec by extrapolating in Fig. 25, because the amplitude in the prototype is, $2\eta_{0p}=62.5\sim100$ cm, for this amplitude, $2\eta_{0m}=0.5\sim0.8$ cm. Since the velocity scale is, $u_r=11.2$, the velocity of flow in the model is, $u_m=8\sim10.7$ cm/sec for this value, $u_p=90\sim120$ cm/sec. This value, $u_m=8\sim10.7$ cm, practically coincides with the result obtained when $2\eta_{0m}=0.5\sim0.8$ cm. Therefore, it is considered that the similitude holds good with respect to the velocity of flow.

Assuming that in the prototype the ratios of amplitudes do not depend on the amplitudes (this is valid when the amplitude is between 7 and 45 cm) and that in the model the roughness coefficient is independent on the period, it is concluded that the similitude holds good when such a characteristic Reynolds number, or the velocity of flow, is realized. The experimental data for the frequency response IV～VII were arranged from this point of view.

The validity of this view for the similitude is proved in the case of the semidiurnal tide. To examine the similitude in the case of short period, the experimental results are compared with the results of analysis of Chilean Tsunami. Since the time scale in this experiment is that $t_r=44.7$, the periods of 1, 1.5, 2, and 3 minutes are involved in the range of the period analyzed in the prototype. The experimental values for these periods are

shown in Fig. 23 by circular marks. From this, it is found that, with the exception of the resonating period, the experimental values are in agreement with the prototype. This proves the correctness of the consideration on the similitude.

5. Consideration by simple theoretical model

It is considered that the system composed of a channel and a reservoir has three characteristic periods. One is that of the channel itself, which is the period of the fundamental oscillation in the channel having the nodes at both ends. Another is that of the reservoir itself, which is practically combined by various periods depending on the complexity of its form. The last one is that of the whole system, which is determined by the dimensions of the channel and the reservoir, the same as the preceding two.

Since it was clarified that the effect of the area of the reservoir plays an important role on the frequency response, and in order to understand how it plays its role and why such experimental results were obtained, a theoretical consideration is obtained by using a simplified working model.

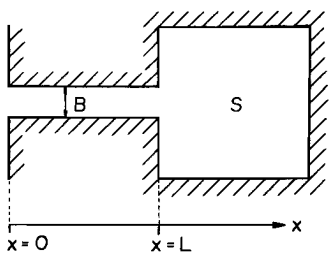

Fig. 57.

For a model, as shown in Fig. 57, composed of a uniform straight channel having a rectangular uniform cross section and a horizontal bottom, and a reservoir of infinite depth, and assuming the linear frictional term, the equations of motion and the continuity are as follows ;

$$\frac{\partial U}{\partial t}+\alpha U+g\frac{\partial \eta}{\partial x}=0 \tag{16}$$

$$\frac{\partial \eta}{\partial t}+\dot{h}\frac{\partial U}{\partial x}=0 \tag{17}$$

where α : the frictional coefficient and η : the displacement of the water level from still water surface. As for the boundary conditions, it is assumed that the oscillation is sinusoidal at $x=0$, and the water spreads throughout the reservoir as soon as it enters, that is,

$$\left.\begin{aligned} &\text{at}\quad x=0: \quad \eta=\eta_0 e^{i\omega t} \\ &\text{at}\quad x=L: \quad \frac{d\eta}{dt}=\frac{Bh}{S}U \end{aligned}\right\} \tag{18}$$

Then the amplitude and maximum mean velocity in the channel are written as follows,

$$\left(\frac{\eta_x}{\eta_0}\right)^2=\Big\{(p^2+q^2)\{\sinh^2 p(L-x)+\sin^2 q(L-x)\}+\frac{B^2}{S^2}\{\sinh^2 p(L-x)+\cos^2 q(L-x)\}+\frac{B}{S}\{p\sinh 2p(L-x)-q\sin 2q(L-x)\}\Big\}\div\Big\{(p^2+q^2)\{\sinh^2 pL+\sin^2 qL\}+\frac{B^2}{S^2}\{\sinh^2 pL+\cos^2 qL\}+\frac{B}{S}\{p\sinh 2pL-q\sin 2qL\}\Big\} \tag{19}$$

$$\left(\frac{U_x}{\eta_0}\right)^2=\frac{g}{h}\frac{1}{\sqrt{1+\frac{\alpha^2}{\omega^2}}}\Big\{(p^2+q^2)\{\sinh^2 p(L-x)+\cos^2 q(L-x)\}+\frac{B^2}{S^2}\{\sinh^2 p(L-x)+\sin^2 q(L-x)\}+\frac{B}{S}\{p\sinh 2p(L-x)+q\sin 2q(L-x)\}\Big\}\div\Big\{(p^2+q^2)\{\sinh^2 pL+\sin^2 qL\}+\frac{B^2}{S^2}\{\sinh^2 pL+\cos^2 qL\}+\frac{B}{S}\{p\sinh 2pL-q\sin 2qL\}\Big\} \tag{20}$$

in which T is the period and

$$\left.\begin{aligned} p^2&=\frac{\omega^2}{2c^2}\left\{\sqrt{1+\frac{\alpha^2}{\omega^2}}-1\right\}, & q^2&=\frac{\omega^2}{2c^2}\left\{\sqrt{1+\frac{\alpha^2}{\omega^2}}+1\right\}\\ \omega&=\frac{2\pi}{T}. & c&=\sqrt{gh}\end{aligned}\right\} \tag{21}$$

These equations can be evaluated when α is assumed. Now, if the frictional term is practically represented by Manning's formula, the coefficient α may be written as follows,

$$\alpha=\frac{gn^2}{h^{4/3}}U \tag{22}$$

and it will be evaluated by using a representative velocity in the experiment.

By using the value of $\alpha(=0.035)$ estimated from the maximum mean velocity, which is obtained from observed surface velocity, and $B/S=5.26\times 10^{-3}$, the equation (19) is numerically calculated. The result is shown in Fig. 58. This corresponds to Fig. 35. Comparing both figures, as it was

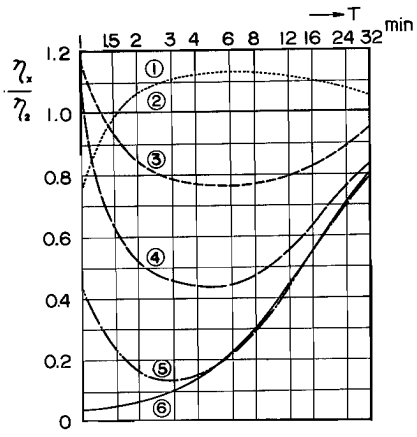

Fig. 58. Theoretical frequency response. Corresponding to Fig. 35.

calculated for simplified model, the theoretical value does not coincide perfectly with the experimental one but the general tendency of the frequency response, for example, excepting at ⑥, the appearence of the minimum between 3 and 8 minutes and the shift of the period which provides the minimum, seems to be considerably similar to the experimental results. The reason why the values of ⑥ at shorter periods do not coincide is because this station does not represent the reservoir.

When the area of the reservoir is infinite ($S\to\infty$), B/S vanishes and the equation (19) becomes;

$$\left(\frac{\eta_x}{\eta_0}\right)^2=\frac{\sinh^2 p(L-x)+\sin^2 q(L-x)}{\sinh^2 pL+\sin^2 qL} \tag{23}$$

In this case, as shown in Fig. 59, the ratios become lower with increase in the period, and then they approach constant values respectively. On the other hand, when S takes a finite value the minimum appears. Therefore, it is understood that the minimum shown in Fig. 35 and 58 takes place because of the finiteness of S, and then it is concluded that the area of the reservoir plays an inportant role on the frequency response of the system composed of a channel and a reservoir. This effect of the area seems to become greater on the longer periods.

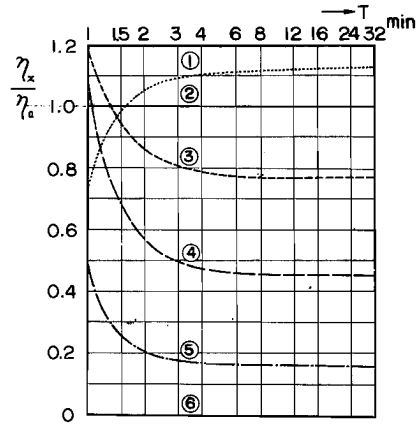

Fig. 59. Theoretical frequency response. When $S\to\infty$.

Since the effect of the reservoir is slight for the oscillation of the period of 1 minute, and the frictional effect is assumed to be negligible because of the shortness of the period, it may be written that $B/S=0$, and $\alpha/\omega\ll 1$. Therefore since $p=0$. $q=\omega/c$, the equation (19) becomes,

$$\frac{\eta_x}{\eta_0}=\frac{\sin\frac{\omega}{c}(L-x)}{\sin\frac{\omega}{c}L}=\frac{\sin\pi\frac{T_0}{T}\left(1-\frac{x}{L}\right)}{\sin\pi\frac{T_0}{T}} \tag{24}$$

where $T_0=2L/\sqrt{gh}$, which is the characteristic period of the channel with both open ends. This equation shows that if $2T_0>T>T_0$, the maximum appears at $\frac{x}{L}=1-\frac{1}{2}\frac{T}{T_0}$ As the characteristic period of this model channel is theoretically 48 sec, the period of 1 minute corresponds to the above mentioned case, that is $2T_0>T>T_0$, and the maximum is expected between ③ and ④. This agreed well with the experimental result.

The result of the numerical calculation of the equation (20) is shown in Fig. 60. The experimental values measured at the location between ④ and ⑤ are shown in full line in the figure. From this figure it is found that the theoretical values coincide with the experimental values in spite of the approximation by the straight uniform channel.

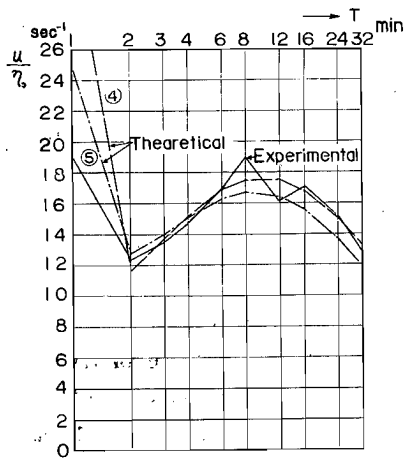

Fig. 60. Velocities of flow of the oscillations of various periods. Experimental and theoretical. Model, with the large reservoir.

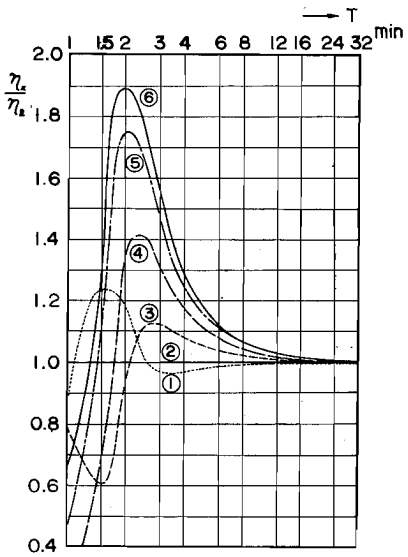

Fig. 61. Theoretical frequency response. Corresponding to Fig. 38.

In the case when the channel was closed, the equation (19) was calculated. The results are shown in Fig. 61, which corresponds with Fig. 38. These figures resemble each other in general tendency, but the maximums appear at different periods. The reason why the theoretical maximum exists

at 2 minutes may be because the resonance occurs at this period. Since the period is short and the area of the reservoir is small, we assume that $\alpha=0$ and $B/S=\infty$, then the equation (19) becomes,

$$\frac{\eta_x}{\eta_0}=\frac{\cos\frac{\omega}{c}(L-x)}{\cos\frac{\omega}{c}L}=\frac{\cos\frac{\pi}{2}\frac{T_0}{T}\left(1-\frac{x}{L}\right)}{\cos\frac{\pi}{2}\frac{T_0}{T}} \tag{25}$$

in which $T_0=4L/\sqrt{gh}$, which is the characteristic period of the closed channel other than before. The theoretical characteristic period in this case is 114 sec. The reason why the experimental characteristic period does not coincide with the theoretical one may be considered to be because the period of the model is lengthened by the energy dissipation at the mouth of the channel and the complexity of the channel form and others. It is interesting to note that the same fact is seen in the prototype for Chilean Tsunami.

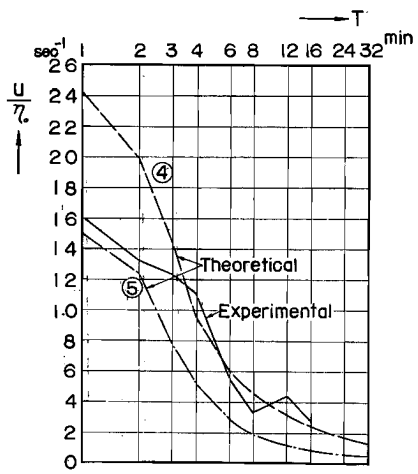

Fig. 62. Velocities of flow of the oscillations of various periods. Experimental and theoretical. Model with the small reservoir.

The theoretical values of the velocities of flow calculated by the equation (20) in this case are shown in Fig. 62. From this it is found that in this case the velocities in the channel become smaller as the period becomes longer. Comparing with Fig. 60, the velocities in shorter periods are the same, but in longer periods they become much weaker when the channel is closed.

Now in order to examine the effect of the dimension of the reservoir, the equation was calculated in wide range of B/S. As the representative location to see the general tendency, the mouth of the channel to the reservoir ($x=L$) was chosen. The results when $\alpha=0.02$, $h=0.045$ m, and $L=15.2$ m, are shown in Fig. 63 by using the period T as the parameter. In this figure the ordinate shows the ratio of the amplitude at $x=L$ to at $x=0$, and the abscissa shows B/S (m^{-1}), which is proportional to the reciprocal of the area of the reservoir, so that the right hand side of this figure ex

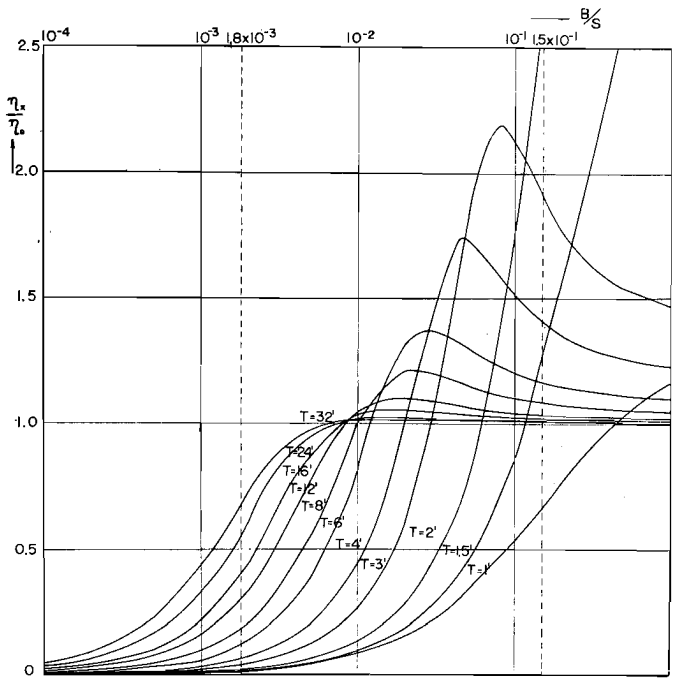

Fig. 63. Effect of the period on the ratio of the amplitudes in the model with the reservoirs of various areas. Theoretical.

peresses the small reservoir. From this figure, it is found that there exists a particular area of the reservoir which resonates to the oscillation of any period in this range. In this figure, broken lines correspond to the precise experiment, that is, $B/S=1.8\times10^{-3}$ corresponds to the present state and $B/S=1.5\times10^{-1}$ to the closed state. This figure was rewritten in Fig. 64 as shown before, in which the abscissa shows the period and the parameter is B/S (m^{-1}).

In this figure, it is found that when the reservoir is infinitely large the ratio of the amplitudes is always zero, and when the reservoir becomes smaller the ratio becomes higher until it takes the maximum. This maximum corresponds with that in the preceding figure and this period is considered the characteristic period of the system. When the reservoir becomes smaller, this period becomes shorter and the maximum value becomes higher. The curves when $B/S=1.8\times10^{-3}$ and $B/S=1.5\times10^{-1}$ in this figure correspond to the curves at ⑥ in Fig. 46 and 48 respectively. The reason why the

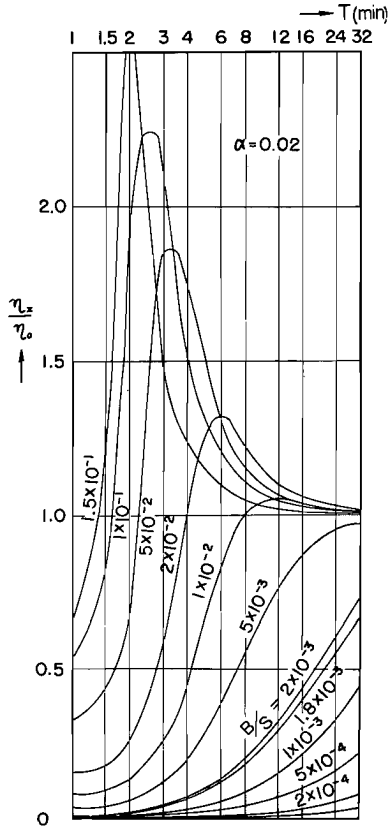

Fig. 64. Effect of the area of the reservoir on the ratio of amplitudes of the oscillations of various periods. Theoretical.

curve at ⑥ in Fig. 46 does not coincide may be the same as the result of the preliminary experiment. In the case of Fig. 48 the theoretical value does not coincide with the experimental one the same as before.

When the reservoir becomes much smaller, the characteristic period becomes much shorter and the maximum value becomes much higher until it turns into the bay oscillation.